Tetragonal tungsten bronze/barium hexaferrite room-temperature multiferroic composite ceramics

Thameur Hajlaoui, Mohsen Elain Hajlaoui, Michaël Josse, Essebti Dhahri, Alain Pignolet

Tetragonal tungsten bronze/barium hexaferrite room temperature multiferroic composite ceramics

Thameur Hajlaoui[1], Mohsen Elain Hajlaoui[2], Michaël Josse[3], Essebti Dhahri[2], Alain Pignolet[1]

[1]Institut National de la Recherche Scientifique – Centre Énergie, Matériaux et Télécommunications, 1650 Boulevard Lionel-Boulet, Varennes, Québec, J3X 1S2, Canada

[2]Laboratory of Applied Physics, Faculté des Sciences de Sfax, Université de Sfax, B.P. 1171, Sfax 3000, Tunisia

[3]Univ. Bordeaux, ICMCB, UPR 9048, F-33600 Pessac, France

Corresponding author: Thameur Hajlaoui (thameur.hajlaoui@emt.inrs.ca)

Abstract

The spontaneously formed multiferroic composite based on tetragonal tungsten bronze structure was successfully synthesized in the form of ceramics by the solid state reaction. The crystallization of the ceramics in the tetragonal tungsten bronze structure $Ba_2SmFeNb_4O_{15}$ and the presence of a secondary magnetic phase of barium hexaferrite $BaFe_{12}O_{19}$ were established by structural investigation. The hysteresis behavior describing the polarization as a function of an applied electric field and the high ferroelectric Curie temperature ≈ 417 K evidenced the room temperature ferroelectric properties of the synthesized material. While the piezoelectric coefficients were determined to be around 1.3 pm/V, the microscopic polar domains of the composite ceramics were established by microelectromechanical study. The hysteresis loops of the magnetization versus magnetic field and the high magnetic transition temperature ≈ 590 K evidenced the ferromagnetic properties of the secondary and its presence at room temperature. Moreover, the spatial distribution of the magnetic domains was determined microscopically. In this study, not only the multiferroic properties of the $Ba_2SmFeNb_4O_{15}/BaFe_{12}O_{19}$ composites have been studied and presented, but the distribution of the polar and magnetic properties was locally investigated as well.

Keywords: composite; room temperature multiferroic; electromechanical properties; polar domains; magnetic domains

Article Highlights

- Multiferroic multifunctional composite tetragonal tungsten bronze/barium hexaferrite ceramics are synthesized.
- Ferroelectric and magnetic transition temperatures were determined by dielectric and magnetic measurements, respectively.
- The spatial distribution of the polar and magnetic domains are demonstrated at room temperature.

Declarations

Funding: this research was funded by the Natural Sciences and Engineering Research Council of Canada (NSERC) Individual Discovery Grant # RGPIN 261662.

Conflicts of interest/Competing interests: no conflict related to this work.

Availability of data and material: not applicable.

Code availability: not applicable.

Introduction

Recently, multiferroic/multifunctional materials have attracted the interest of scientists due to their rich properties and their potential use in a wide range of advanced applications [1–5]. In particular, the coexistence of ferroelectric and ferromagnetic properties in these materials makes them promising candidates for data storage devices [6,7], including new generations of non-volatile integrated memories [8–10]. In order to overcome the issue of the scarcity of single phase multiferroic materials, especially at the ambient temperature and above, several strategies have been adopted in order to develop new multiferroic materials at room temperature [11–14]. One of the most efficient is to synthesize composites materials formed by ferroelectric and ferromagnetic phases, which allows the use of a large variety of ferroelectric/piezoelectric and magnetic material couples, having both good ferroelectric and good ferromagnetic properties [5,15–18]. An important issue with composites is the chemical compatibility of the targeted phases, and the formation of secondary phases (or of interphases) can be complex and challenging [19,20].

Tetragonal tungsten bronzes (TTB) are a class of materials having a crystal structure consisting of a framework of corner-sharing octahedra connected in such a way that different channels with different shapes (triangular, square and pentagonal channels) are formed. These channels are all oriented along the short crystallographic c-axis, and can be filled, partially filled or empty. Such a crystal structure with a large number of cationic and anionic sites allows for the synthesis of large variety of composites and dopings, resulting in a fine control and a large enhancement of the functional properties of the synthesized material [21–24]. Crystalizing in this particular structure, the ferroelectric tetragonal tungsten bronze $Ba_2LnFeNb_4O_{15}$ (TTB-Ln), with Ln being a Lanthanide, have been shown to exhibit a particular behavior, namely the generation *in-situ* of ferromagnetic barium hexaferrite ($BaFe_{12}O_{19}$: BaFO), during the proper sintering of the ferroelectric matrix [21,25,26]. This processes therefore produces a *spontaneously forming* multiferroic ceramic composite and overcomes any chemical compatibility issue that are common with conventional composites.

For complete understanding of the multiferroic properties and their microscopic distribution, this contribution reports a complementary investigation of the ferroelectric and ferromagnetic properties of TTB-Sm/BaFO composite ceramics synthesized by solid state reaction [21]. By studying the dielectric coefficients and the magnetization versus the temperature, we determined the ferroelectric and the ferromagnetic transition temperatures, which confirms the room temperature multiferroic nature of the composite. In addition, we used

microelectromechanical investigations to study the polar domains at the ceramics surface and determine their piezoelectric coefficients. We also studied the magnetic response at the microscopic level, and we determined the spatial distribution of the magnetic secondary phase.

Materials and methods

Tetragonal tungsten bronze multiferroic composite ceramics were prepared by solid state reaction method. The precursors $BaCO_3$, Fe_2O_3, Nb_2O_5 and Sm_2O_3 (having a purity higher than 99%) were mixed by mechanical grinding and pressed under uni-axial pressure of 4 ton/cm² into cylindrical pellets with a diameter of 8 mm and a thickness around 1.2 mm before being sintered at 1300 °C during 4 hours in air. The ceramics crystallization and phase identification were characterized at room temperature by X-ray diffraction collected using a 4-circle X-ray diffractometer (PANalytical X-Pert PRO MRD). In order to prepare the samples for ferroelectric and dielectric measurements, we deposited, on each side of the pellet, a 200 nm thick layer of gold by using thermal evaporation under vacuum giving disk-shaped electrodes of 6 mm diameter each. Dielectric characteristics were performed with Wayne–Kerr 6425 component analyzer under dry helium at frequencies ranging from 10^3 to 10^6 Hz. The electric field dependence of the polarization was measured using an analogical Sawyer-Tower circuit with compensation of stray capacitances and resistances. The microstructure, the local electromechanical properties and the microscopic magnetic response were characterized by an atomic force microscope (AFM) using a DI-enviroscope AFM (Bruker, Santa Barbara, CA). To image and manipulate the ferroelectric polarization of the samples at the nanoscale, we used piezoresponse force microscopy (PFM) and we applied a voltage of 3 V at 20 kHz between the conductive tip and a silver past bottom electrode. The surface-induced piezoelectric vibrations were detected using a lock-in amplifier from Signal Recovery (model 7265, Wokingham, UK). Magnetic force microscopy (MFM) was performed to investigate the local magnetic response of the samples. The microscopic measurements were carried out with conductive/magnetic tips, having a Co/Cr coating (MESP from Bruker, Santa Barbara, CA), thus suitable for both electric and magnetic measurements. At the macroscopic level, the variation of the magnetization as a function of temperature and as a function of an applied magnetic field were studied using an EV9 Vibrating Sample Magnetometer (VSM) produced by Microsense (Lowell, MA, USA).

Results and discussion

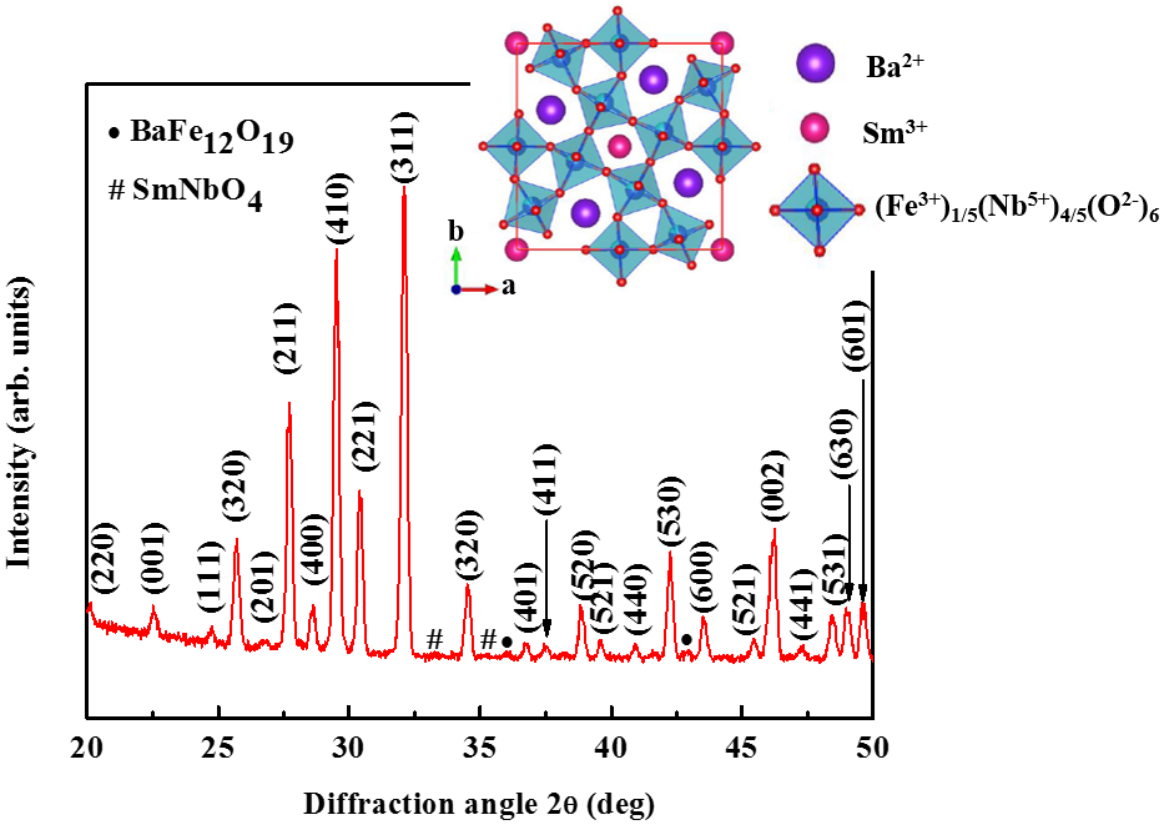

Fig. 1: X-ray diffractogram of the synthesized TTB-Sm/BaFO ceramic composite: in addition to the diffraction peaks of the TTB-Sm (shown with their Miller indices), the peaks of the secondary phases $BaFe_{12}O_{19}$ and $SmNbO_4$ are shown with the symbols (•) and (#), respectively. The inset displays a unit cell of TTB-Sm, indicating the different channels with pentagonal (filled with Ba^{2+}), square (filled with Sm^{2+}) and triangular (empty) shapes and the positions of the different ions.

Figure 1 shows the X-ray diffractogram of the composite ceramics. The diffraction peaks shown with the Miller indices are attributed to the principal phase TTB-Sm according to the reference file JCPDS 00-059-0425, confirming that the principal phase crystallizes in the tetragonal system with the tungsten bronze structure belonging to with the space group P4/mbm. The coherent domain size is determined to be around 35 nm using Scherrer's formula [27], which is in accordance with [28]. A sketch of the TTB-Sm crystal structure seen along the crystallographic c-axis is drawn using the software VESTA and the crystallographic data provided in [21,29], is shown in the inset of **Figure 1**. In this structure, the barium ions occupy the pentagonal sites, the samarium ions are contained in the square sites, while the triangular sites are kept empty. The Fe^{3+} and Nb^{5+} metal ions are statistically distributed within oxygen octahedral, which are responsible to the appearance of the

ferroelectric polarization [21,26]. Moreover, $SmNbO_4$ phase (#) is always detected, due to the limited structural distortions of the TTB phase, which results only in a partial accommodation of the samarium ions [21,26]. The remaining ions interact with a small amount of niobium and oxygen to form the Fergusonite phase. In order to maintain electrical neutrality, iron ions can only be partially incorporated in the TTB framework and the excess portion of iron oxide reacts with a small amount of barium oxide in order to form the BaFO phase (•) [21,25,30]. Although the fergusonite phase does not present ferroic properties at room temperature, its presence is required to trigger the formation of the magnetic phase of hexaferrite. In addition, the formation of the magnetic BaFO phase is very desirable because of the large use of this phase in several applications, such magnetic recording and microwave applications [31–33].

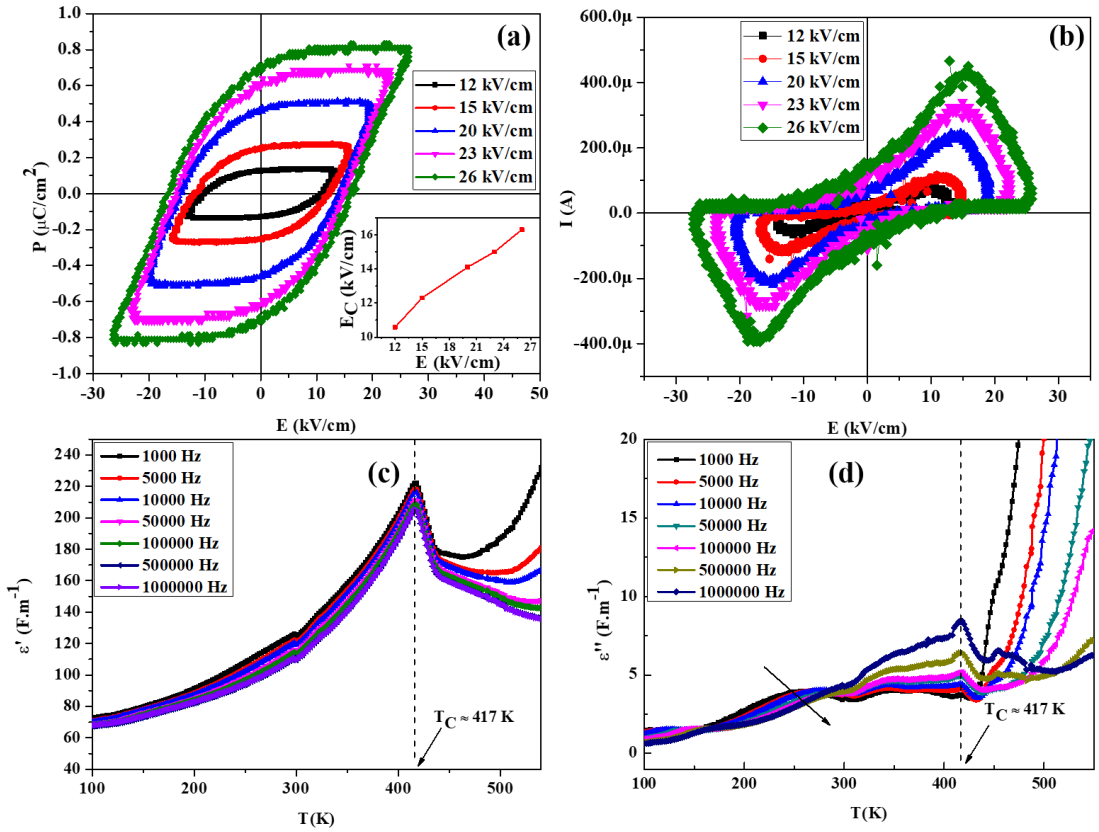

Fig. 2: Room temperature ferroelectric properties of the synthesized ceramics: (a) and (b) represent the variation of the polarization and switching current as a function of an applied voltage, respectively, for various electric field amplitudes ranging from 12kV/cm to 26 kV/cm. The inset of (a) shows the variation of the coercive field as a function of the maximum electric field applied. Variation of the dielectric permittivity as a function of temperature and frequency: (c) real part and (d) imaginary part of the dielectric permittivity.

To investigate the ferroelectric properties in the prepared ceramics, we studied the polarization hysteresis loops obtain by applying an electric field of various amplitude varying form 12 kV/cm to 26 kV/cm. The dependence on the electric field of the global polarization (P-E) and the current (I-E) across a pellet of ceramic sandwiched between two gold electrodes is shown in **Figure 2(a)** and **2(b)**, respectively. The hysteresis behavior that describes the variation of the polarization in the sample submitted to an electric field shows the reversible switching of the polarization between two opposite states, evidencing the ferroelectric properties of the composite. Even after applying the highest electric field that can be reached by our system without causing a breakdown across the ceramic (E_{max} = 26 kV/cm), the saturation polarization was not reached and the maximum measured value of the polarization is $P_{max} \approx 0.8\ \mu C\ cm^{-2}$. The electric coercive field (E_C) is plotted as a function of the maximum electric field applied as shown in the inset of the **Figure 2(a)**, depicts an increase of E_C while increasing the applied electric field to reach a maximum measured value of $\approx 16.3\ kV\ cm^{-1}$. As known for ferroelectric materials, the increase of E_C is mainly related to the movement of ferroelectric domain walls, which depend on the applied electric field. The variation of the switching current as a function of the applied electric field is represented in **Figure 2(b)**. The presence of two antisymmetric peaks with respect to the current axis gives indication on the coercive field and proves the switching of the ferroelectric polarization. While the variation of the position of the current peaks with the applied field is related to the variation of the coercive field, the increase of its amplitude is related to the increase of the maximum of the measured polarization.

The temperature dependence of the real part of the permittivity ε' at various frequencies ranging from 10^3 Hz to 10^6 Hz has been studied and the results are displayed in **Figure 2(c)**. The real part of the permittivity of the TTB-Sm solid solution possesses a relatively narrow peak at a temperature around 417 K. The position of this peak indicates that the ceramic undergoes a paraelectric-ferroelectric phase transition at a Curie temperature around $T_C \approx 417$ K. The unchanged position of the peak while increasing the frequency of the measurement is a solid evidence to the ferroelectric nature of the ceramic, confirming the results of the P-E hysteresis loops shown in **Figure 2(a)**. We found that Curie temperature determined here by dielectric measurements is slightly higher than that determined in [21] ($T_C \approx 405$ K). In the paraelectric region ($T>T_C$), the real part of the permittivity does not obey the linear behavior expected from the Curie-Weiss law in the paraelectric state, as a change of slope is obvious around 430 K. This can be related to the behavior observed in the $Ba_2NbFe(Nb_{1-x}Ta_x)_4O_{15}$ solid solution, and to the existence of a metastable ferroelectric phase that appear as a general feature in this TTB series [23,34].

The temperature dependence of the imaginary part of the dielectric permittivity (ε'') at various frequencies has also been measured and is depicted in **Figure 2(d)**. A peak having a maximum position independent to the frequency at T = T_C is obtained, which is clearly related to the paraelectric-ferroelectric phase transition. Moreover, a second dielectric anomaly is observed at lower temperature of around 250 K, suggesting a second phase transition at reduced temperature that can be related to the recurrent ferroelectric to relaxor crossovers observed in this series [21,23,35]. The presence of a very wide peak which is extending over a large frequency range indeed indicates that the low temperature transition is a relaxor-like ferroelectric transition [36,37]. Finally, the imaginary part of the permittivity increases drastically at high temperatures (T> 432 K), which reflects the presence of extrinsic contributions related to the establishment of a significant electrical conductivity [38]. This dielectric investigation, however, confirms that the studied ceramics are ferroelectric at room temperature.

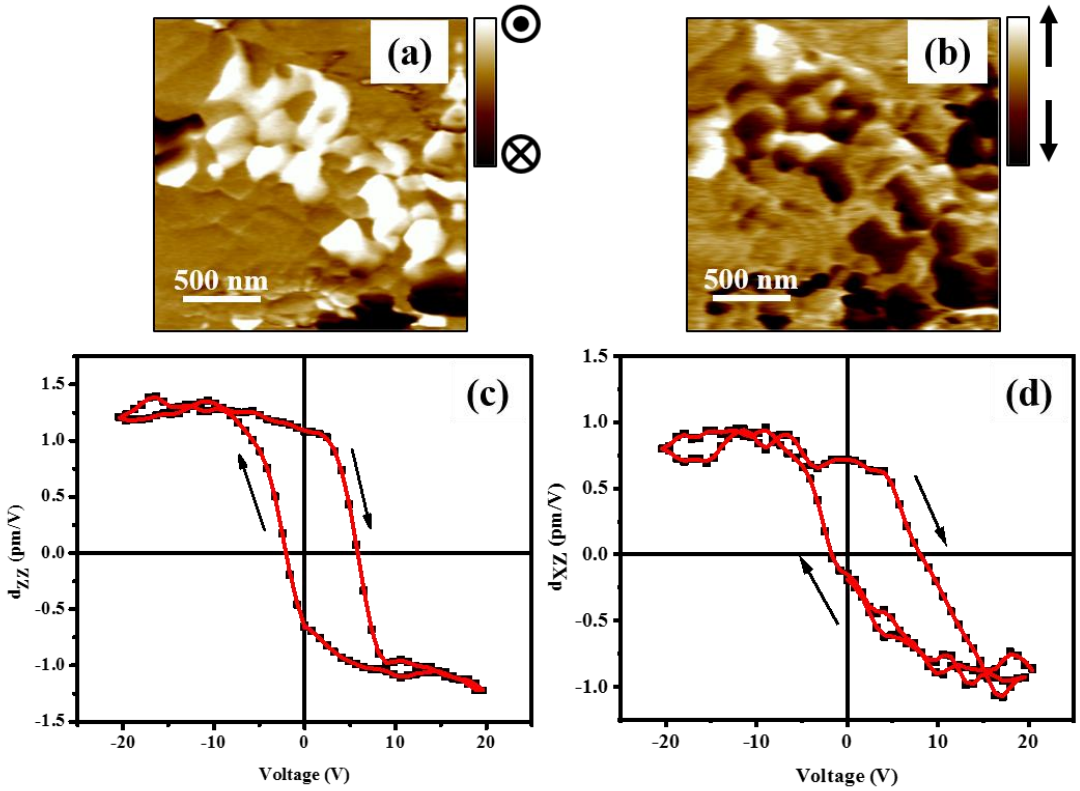

Fig. 3: Microscopic electromechanical properties of TTB-Sm ceramics investigated at room temperature: (a) and (b) show respectively the out-of-plane and the in-plane piezoelectric responses detected at the ceramics surface. (c) and (d) represent the applied voltage dependence of the out-of-plane and the in-plane piezoelectric coefficients, respectively.

In order to investigate the microelectromechanical properties of the studied ceramics and get space-resolved information about their ferroelectric properties at room temperature, piezoelectric force microscopy was used. The out-of-plane and the in-plane piezoelectric responses (mixed signal, i.e. amplitude × cos(phase)) are shown in **Figure 3(a)** and **3(b)**, respectively. First, the bright and dark contrasts in **Figure 3(a)** are respectively attributed to polar regions where the out-of-plane component of the polarization is oriented upward (⦿) and downward (⊗) perpendicular to the plane of the image, i.e. the surface of the ceramic sample. Second, the bright and dark contrasts observed in **Figure 3(b)** indicate the presence of polar regions where the polarization is lying in the plane of the sample surface and oriented in opposite directions, as depicted by the arrows (↑↓). These contrasts evidence the out-of-plane and the in-plane piezoelectric vibrations, thus the piezoelectric properties of the studied material.

In order to get more information about the local ferroelectric and piezoelectric properties of the studied system at room temperature, we evaluated the variation of the longitudinal (d_{ZZ}) and the transversal (d_{XZ}) piezoelectric coefficients [39,40] by cycling an external voltage via the PFM tip fixed above selected locations on the sample surface. The dependence of d_{ZZ} and d_{XZ} on the applied bias pulse is described by a hysteresis loop as shown in **Figure 3(c)** and **3(d)**, respectively. The well-saturated character of the hysteresis curves proves that the polarization can be reversibly switched between two opposite stable states, which clearly confirms the ferroelectric nature of the material. This result suggests that this material could possibly be used for memory devices that require the polarization to switch between two states with an angle of 180° [41]. The maximum value of piezoelectric coefficients d_{ZZ} and d_{XZ} are estimated at 1.3 pm/V and 1 pm/V, respectively. The difference of coercive voltages in both positive and negative directions is related to the fact that the top electrode (the AFM/PFM tip) has both a very different geometry and a different composition than the continuous bottom electrode [42]. The average coercive voltage is similar in both cases of piezoelectric coefficients, which is estimated at ≈ 4.5 V.

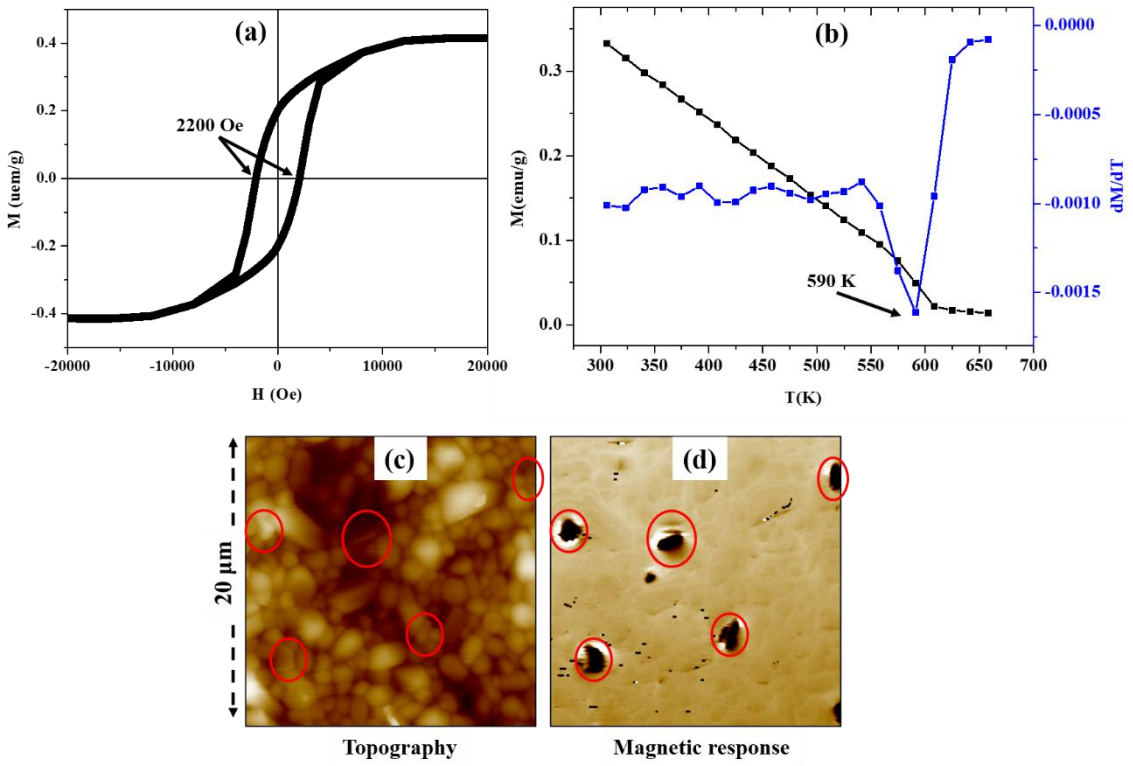

Fig. 4: Investigation, at the macroscopic and microscopic scales, of the magnetic properties of TTB-Sm/BaFO ceramic composite. (a) Represents the room temperature variation of the magnetization as a function of an applied magnetic field, while (b) depicts the variation of the magnetization as a function of temperature. (c) and (b) represent respectively the topography and the microscopic magnetic response of the sample surface measured at room temperature, showing the magnetic domains distribution at the ceramic surface.

In order to determine the nature and the spatial distribution of the magnetic phase embedded in the ferroelectric matrix, the magnetic properties have been studied at macroscopic and microscopic levels, as shown in **Figure 4**. First, the hysteresis loop describing the variation of the macroscopic magnetization as a function of an applied magnetic field was studied at room temperature as depicted in **Figure 4(a)**, evidencing of the presence of a room temperature ferromagnetic ordering in the studied TTB-Sm/BaFO ceramic composite. The magnetic coercive field (H_C) measured to be around 2200 Oe (0.22 Tesla) corresponds to the magnetic coercive field of the *in-situ* forming 'hard' magnetic phase within the ferroelectric matrix TTB-Sm [21,26,30]. The magnetization as a function of temperature is studied and is depicted in **Figure 4(b)**, which shows a decrease of magnetization and a transition from a ferromagnetic to a paramagnetic phase when increasing the temperature. For accurate determination of the transition temperature, the derivation of the magnetization is plotted as a function of the temperature (**Figure 4(b)**), and its minimum is obtained at 590 K, which is ascribed to the magnetic transition

temperature of the TTB-Sm/BaFO samples. The high transition temperature together with the large magnetic coercive field are in concordance with the magnetic signature of BaFO phase. This result, together with the ferroelectric behavior discussed above, prove that these ceramics are multiferroic at room temperature.

To determine the spatial distribution of the magnetic phase at the sample surface, magnetic force microscopy was used. The surface topography and the magnetic response measured at room temperature are shown in **Figure 4(c)** and **4(d)**, respectively. The image of the topography shows that the microstructure of the ceramic is formed by a grain structure of lateral dimensions varying from 0.8 μm to 3 μm, giving rise to a roughness of about RMS ≈ 250 nm. The presence of domains with dark contrast in the image of the magnetic response reveals the presence of magnetic domains within a non-magnetic matrix (the ferroelectric matrix TTB-Sm), at locations indicated by the red circles in **Figure 4(c)** and **4(d)**. A careful comparison between these two images indicates the absence of any correlation between the topography and the magnetic response, confirming that the contrasts observed in **Figure 4(c)** are solely due to the presence of magnetic domains at or near the sample surface. The average size of the magnetic domains (which we associate with the BaFO phase) is around 1.38 μm, indicating that these magnetic domains are probably formed by several grains of BaFO. This proves that magnetic domains are indeed spontaneously formed within the ferroelectric matrix during its thermal treatment, and demonstrates that their magnetic properties can be experimentally observed, giving rise to room temperature multiferroic composite in the form of ceramics.

Conclusion

Multiferroic composite ceramics TTB-Sm/BaFO were synthesized and their multifunctional properties were investigated. The ferroelectric and the magnetic phase transition temperatures were determined to be 417 K and 590 K, respectively. In addition, ferroelectric and ferromagnetic hysteresis loops were measured at room temperature. The microelectromechanical characterization confirmed the presence of ferroelectric properties down to nanoscale and allowed the determination of the piezoelectric coefficients. The formation of the magnetic phase in the form of microdomains was confirmed by studying the magnetic response of the ceramic at the microscopic level. In this study, not only the multiferroic properties of the TTB-Sm/BaFO composite ceramics have been investigated, but the distribution of the polar and magnetic properties was locally studied as well. Finally, the coexistence of the polar and magnetic domains in the same material suggests the investigation of possible couplings between these domains (magnetoelectric coupling) as a prospective for this study.

References

[1] N. a Spaldin, S. Cheong, R. Ramesh, Multiferroics : Past , present , and future feature, Phys. Today. 63 (2010) 38–43. https://doi.org/10.1063/1.3502547.

[2] C. Lu, W. Hu, Y. Tian, T. Wu, Multiferroic oxide thin films and heterostructures, Appl. Phys. Rev. 2 (2015) 021304. https://doi.org/10.1063/1.4921545.

[3] R. Ramesh, N.A. Spaldin, Multiferroics: progress and prospects in thin films, Nat. Mater. 6 (2007) 21–29. https://doi.org/10.1038/nmat1805.

[4] W. Eerenstein, N.D. Mathur, J.F. Scott, Multiferroic and magnetoelectric materials, Nature. 442759 (2006) 759–765. https://doi.org/10.1038/nature05023.

[5] C.W. Nan, M.I. Bichurin, S. Dong, D. Viehland, G. Srinivasan, Multiferroic magnetoelectric composites: Historical perspective, status, and future directions, J. Appl. Phys. 103 (2008) 1–35. https://doi.org/10.1063/1.2836410.

[6] N.A. Spaldin, R. Ramesh, Advances in magnetoelectric multiferroics, Nat. Mater. 18 (2019) 203–212. https://doi.org/10.1038/s41563-018-0275-2.

[7] S.H. Baek, H.W. Jang, C.M. Folkman, Y.L. Li, B. Winchester, J.X. Zhang, Q. He, Y.H. Chu, C.T. Nelson, M.S. Rzchowski, X.Q. Pan, R. Ramesh, L.Q. Chen, C.B. Eom, Ferroelastic switching for nanoscale non-volatile magnetoelectric devices, Nat. Mater. 9 (2010) 309–314. https://doi.org/10.1038/nmat2703.

[8] J. Shen, J. Cong, D. Shang, Y. Chai, S. Shen, K. Zhai, Y. Sun, A multilevel nonvolatile magnetoelectric memory, Sci. Rep. (2016) 1–6. https://doi.org/10.1038/srep34473.

[9] A. Roy, R. Gupta, A. Garg, Multiferroic memories, Adv. Condens. Matter Phys. 2012 (2012) 1–12. https://doi.org/10.1155/2012/926290.

[10] J.F. Scott, Multiferroic memories, Nat. Mater. 6 (2007) 256–257.

[11] R. Nechache, L.-P. Carignan, L. Gunawan, C. Harnagea, G.A. Botton, D. Ménard, A. Pignolet, Epitaxial thin films of multiferroic Bi2FeCrO6 with B-site cationic order, J. Mater. Res. 22 (2011) 2102–2110. https://doi.org/10.1557/jmr.2007.0273.

[12] D.A. Sanchez, N. Ortega, A. Kumar, G. Sreenivasulu, R.S. Katiyar, J.F. Scott, D.M. Evans, M. Arredondo-Arechavala, A. Schilling, J.M. Gregg, Room-temperature single phase multiferroic magnetoelectrics: Pb(Fe, M) x(Zr,Ti)(1-x)O3 [M = Ta, Nb], J. Appl. Phys. 113 (2013) 1–7. https://doi.org/10.1063/1.4790317.

[13] H.J. Zhao, W. Ren, Y. Yang, J. Iniguez, X.M. Chen, L. Bellaiche, Near room-temperature multiferroic materials with tunable ferromagnetic and electrical properties, Nat. Commun. (2014) 1–7. https://doi.org/10.1038/ncomms5021.

[14] J.F. Scott, Room-temperature multiferroic magnetoelectrics, NPG Asia Mater. 5 (2013) 1–11. https://doi.org/10.1038/am.2013.58.

[15] K.P. Jayachandran, J.M. Guedes, H.C. Rodrigues, Solutions for maximum coupling in multiferroic magnetoelectric composites by material design, Sci. Rep. (2018) 1–9. https://doi.org/10.1038/s41598-018-22964-9.

[16] J. Ma, J. Hu, Z. Li, C.W. Nan, Recent progress in multiferroic magnetoelectric composites: From bulk to thin films, Adv. Mater. 23 (2011) 1062–1087. https://doi.org/10.1002/adma.201003636.

[17] D. Ai, J. Xu, C. Huang, W. Zhou, L. Zhao, J. Sun, Q. Wang, Synthesis and magnetoelectric properties of multiferroic composites of lead lanthanum zirconate titanate and mesoporous cobalt ferrite, Scr. Mater. 136 (2017) 29–32. https://doi.org/10.1016/j.scriptamat.2017.04.003.

[18] R. Gao, X. Qin, Q. Zhang, Z. Xu, Z. Wang, C. Fu, G. Chen, X. Deng, W. Cai, A comparative study of the dielectric, ferroelectric and anomalous magnetic properties of Mn0.5Mg0.5Fe2O4/Ba0.8Sr0.2Ti0.9Zr0.1O3 composite ceramics, Mater. Chem. Phys. 232 (2019) 428–437. https://doi.org/10.1016/j.matchemphys.2019.05.016.

[19] V. V. Laguta, C. Elissalde, M. Maglione, A.M. Artemenko, V. Chlan, H. Stepankova, Y. Zagorodniy, Crystal structure transformations induced by surface stresses in BaTiO3 and BaTiO3@SiO2 nanoparticles and ceramics, Phase Transitions. 88 (2015) 761–775. https://doi.org/10.1080/01411594.2014.996852.

[20] U.C. Chung, D. Michau, C. Elissalde, S. Li, A. Klein, M. Maglione, Evidence of diffusion at BaTiO3/silicon interfaces, Thin Solid Films. 520 (2012) 1997–2000. https://doi.org/10.1016/j.tsf.2011.09.055.

[21] M. Josse, O. Bidault, F. Roulland, E. Castel, A. Simon, D. Michau, R. Von der Muhll, O. Nguyen, M. Maglione, The Ba2LnFeNb4O15 “tetragonal tungsten bronze”: Towards RT composite multiferroics, Solid State Sci. 11 (2009) 1118–1123. https://doi.org/10.1016/j.solidstatesciences.2009.02.015.

[22] S.S. Aamlid, S.M. Selbach, T. Grande, The Effect of Cation Disorder on Ferroelectric Properties of SrxBa1−xNb2O6 Tungsten Bronzes, Materials (Basel). 12 (2019) 1–11. https://doi.org/10.3390/ma12071156.

[23] M. Josse, P. Heijboer, M. Albino, F. Molinari, F. Porcher, R. Decourt, D. Michau, E. Lebraud, P. Veber, M. Velazquez, M. Maglione, Original crystal-chemical behaviors in (Ba,Sr)2Ln(Fe,Nb,Ta)5O15 tetragonal tungsten bronze: Anion-driven properties evidenced by cationic substitutions, Cryst. Growth Des. 14 (2014) 5428–5435. https://doi.org/10.1021/cg5006049.

[24] Z. Yang, L. Wei, B. Yang, P. Yang, J. Li, Effects of A-site cations on the electrical behaviors in (Sr1-xCax)2.1Na0.8Nb5O15 tungsten bronze ferroelectrics, Mater. Chem. Phys. 243 (2020) 122006. https://doi.org/10.1016/j.matchemphys.2019.122006.

[25] F. Roulland, M. Josse, E. Castel, M. Maglione, Influence of ceramic process and Eu content on the composite multiferroic properties of the Ba6-2xLn2xFe1+xNb9-xO30 TTB system, Solid State Sci. 11 (2009) 1709–1716. https://doi.org/10.1016/j.solidstatesciences.2009.05.031.

[26] E. Castel, M. Josse, F. Roulland, D. Michau, L. Raison, M. Maglione, In-situ formation of barium ferrite in iron-doped "tetragonal tungsten bronze": Elaboration of room temperature multiferroic composites, J. Magn. Magn. Mater. 321 (2009) 1773–1777. https://doi.org/10.1016/j.jmmm.2009.02.010.

[27] P. Scherrer, Bestimmung der Größe und der inneren Struktur von Kolloidteilchen mittels Röntgenstrahlen, Göttinger Nachrichten Math. Phys. 2 (1918) 98–100.

[28] T. Hajlaoui, C. Harnagea, D. Michau, M. Josse, A. Pignolet, Highly oriented multiferroic Ba 2 NdFeNb 4 O 15 -based composite thin films with tetragonal tungsten bronze structure on silicon substrates, J. Alloys Compd. 711 (2017) 480–487. https://doi.org/10.1016/j.jallcom.2017.04.051.

[29] V. Bovtun, S. Kamba, S. Veljko, D. Nuzhnyy, K. Knížek, M. Savinov, J. Petzelt, Relaxor-like behavior of lead-free Sr2LaTi2Nb 3O15 ceramics with tetragonal tungsten bronze structure, J. Appl. Phys. 101 (2007) 1–7. https://doi.org/10.1063/1.2713094.

[30] M. Josse, Des fluorures aux ferroïques, l'empire de la cristallochimie, Université de Bordeaux, 2012. https://tel.archives-ouvertes.fr/tel-00842197/.

[31] Z. CHEN, F. YANG, Barium hexa-ferrite technology for MAMIR and advanced magnetic recording applications, 14/799,313, 2017.

[32] M.P. Sharrock, L.W. Carlson, Application of barium ferrite particles in advanced recording media, IEEE Trans. Magn. 31 (1995) 2871–2876. https://doi.org/10.1109/20.490177.

[33] S. Ozah, N.S. Bhattacharyya, Nanosized barium hexaferrite in novolac phenolic resin as microwave absorber for X-band application, J. Magn. Magn. Mater. 342 (2013) 92–99. https://doi.org/10.1016/j.jmmm.2013.04.050.

[34] M. Albino, P. Heijboer, F. Porcher, R. Decourt, P. Veber, M. Maglione, M. Josse, Metastable ferroelectric phase and crossover in the Ba2NdFeNb4-xTaxO15 TTB solid solution, J. Mater. Chem. C. 6 (2018) 1521–1534. https://doi.org/10.1039/c7tc04742h.

[35] E. Castel, M. Josse, D. Michau, M. Maglione, Flexible relaxor materials: Ba2PrxNd1− xFeNb4O15 tetragonal tungsten bronze solid solution, J. Phys. Condens. Matter. 21 (2009) 452201. https://doi.org/10.1088/0953-8984/21/45/452201.

[36] A. Peláiz-Barranco, F. Calderón-Piñar, O. García-Zaldívar, Y. González-Abreu, Relaxor Behaviour in Ferroelectric Ceramics Chapter, in: Adv. Ferroelectr., InTech, 2016: pp. 85–107. https://doi.org/10.5772/47751.hancement.

[37] L.E. Cross, Ferroelectrics Relaxorferroelectrics : An overview, Ferroelectrics. 151 (1994) 305–320.

[38] T.F. Zhang, X.G. Tang, Q.X. Liu, S.G. Lu, Y.P. Jiang, X.X. Huang, Q.F. Zhou, Oxygen-vacancy-related relaxation and conduction behavior in (Pb1-xBax)(Zr0.95Ti0.05)O3 ceramics, AIP Adv. 4 (2014) 1–11. https://doi.org/10.1063/1.4900610.

[39] C. Harnagea, C.V. Cojocaru, A. Pignolet, Local ferroelectric switching properties in BiFeO3 microstructures and their piezomagnetic response, MRS Proc. 902 (2005) 1–6. https://doi.org/10.1557/PROC-0902-T10-57.

[40] C. Harnagea, C. V Cojocaru, R. Nechache, O. Gautreau, F. Rosei, A. Pignolet, Towards ferroelectric and multiferroic nanostructures and their characterisation, Int. J. Nanotechnol. 5 (2008) 930–962.

[41] H. Palneedi, V. Annapureddy, S. Priya, J. Ryu, Status and Perspectives of Multiferroic Magnetoelectric Composite Materials and Applications, Actuators. 5 (2016) 1–31. https://doi.org/10.3390/act5010009.

[42] T. Hajlaoui, L. Corbellini, C. Harnagea, M. Josse, A. Pignolet, Enhanced ferroelectric properties in multiferroic epitaxial Ba2EuFeNb4O15 thin films grown by pulsed laser deposition, Mater. Res. Bull. 87 (2017) 186–192. https://doi.org/10.1016/j.materresbull.2016.11.033.